DEVELOPMENTAL BIOLOGY

Bioelectric signaling and the control of cardiac cell identity in response to mechanical forces

Hajime Fukui[1,2], Renee Wei-Yan Chow[1], Jing Xie[3], Yoke Yin Foo[4], Choon Hwai Yap[4,5], Nicolas Minc[3], Naoki Mochizuki[2], Julien Vermot[1,5]*

Developing cardiovascular systems use mechanical forces to take shape, but how ubiquitous blood flow forces instruct local cardiac cell identity is still unclear. By manipulating mechanical forces in vivo, we show here that shear stress is necessary and sufficient to promote valvulogenesis. We found that valve formation is associated with the activation of an extracellular adenosine triphosphate (ATP)–dependent purinergic receptor pathway, specifically triggering calcium ion (Ca^{2+}) pulses and nuclear factor of activated T cells 1 (Nfatc1) activation. Thus, mechanical forces are converted into discrete bioelectric signals by an ATP-Ca^{2+}-Nfatc1–mechanosensitive pathway to generate positional information and control valve formation.

The cardiovascular system is continuously exposed to mechanical forces such as fluid shear stresses and stretching forces generated by blood flow and heartbeat. In the heart, the mechanotransduction cascade translates forces into cellular biochemical signals in the endocardial cells (EdCs) to shape valves (*1*, *2*). These cell types present unique functional properties and are thought to differentially respond to forces depending on the heart regions to which they belong (*3*, *4*). Here, we examined the ability of mechanical forces to modulate specific endocardial fate toward valvulogenesis. We found that valvular cell identity is directed by mechanical forces through different mechanosensitive pathways: transient receptor potential (TRP)–mediated *klf2a* activation and adenosine triphosphate (ATP)–mediated Ca^{2+} oscillations leading to Nfatc1 signaling in response to local high shear stresses.

Using zebrafish to allow for high-precision control of spatiotemporal mechanical parameters, we analyzed Ca^{2+} dynamic patterns by live imaging of the fluorescent Ca^{2+}-sensor protein GCaMP7a expressed in EdCs using *Tg(fli1a:galff);(uas:GCaMP7a)* (*5*). We found that EdCs displayed Ca^{2+} oscillations almost exclusively in the EdCs of the atrioventricular canal (AVC) that will form the AV valve (Fig. 1, A to C; fig. S1, A to E; and movies S1 and S2) between 32 and 102 hours postfertilization (hpf). To verify that the Ca^{2+} oscillations were associated with valvulogenic differentiation, we searched for the decoder and the effector of Ca^{2+} signaling. Nuclear factor of activated T cells 1 (Nfatc1) is an established Ca^{2+}-sensitive transcription factor known to modulate the endocardial-to-mesenchymal transition and subsequent heart valve morphogenesis (fig. S2, A and B) (*6*–*11*). We generated a Nfat binding element reporter line, *Tg(4xnfbr:d2EGFP)*, which expresses d2EGFP in response to the binding of nuclear-localized Nfat protein (fig. S2, C and D). Nfat reporter expression was observed in EdCs of the AVC from 34 hpf onward (Fig. 1, D and E, and fig. S2E), with a similar time course observed for the Ca^{2+} response (Fig. 1, C and E). We confirmed these results by tracking Nfat nuclear relocalization of an endothelial- and endocardial-specific green fluorescent protein (GFP)–Nfatc1 reporter (fig. S2F). Thus, both spatial and temporal regulation of Ca^{2+} signaling and Nfat activation are features of the valvulogenic EdCs.

To determine whether the observed Ca^{2+} oscillations in EdCs are force responsive, we assessed the Ca^{2+} signals in hearts stopped by MS-222 or p-amino blebbistatin treatment. We found that Ca^{2+} oscillations were abrogated in EdCs when the heart stopped and recovered after the heartbeat was restarted (fig. S3, A to C). Because lower hematocrit affects shear stress and flow profile in the AVC (*12*, *13*), we analyzed the bloodless mutant Vlad Tepes (*gata1a*) (*14*). Both *gata1a* mutants and morphants exhibited fewer Ca^{2+} spikes and a decrease in Nfat activity (fig. S3, D to G). Thus, both Ca^{2+} oscillations and Nfat activation are stimulated in response to mechanical forces generated by the beating heart.

We next changed the mechanical force distribution in the living heart by artificially changing the boundary conditions and thus the flow forces in the system (Fig. 2A). We inserted a 30- to 60-μm-diameter agarose-based magnetic

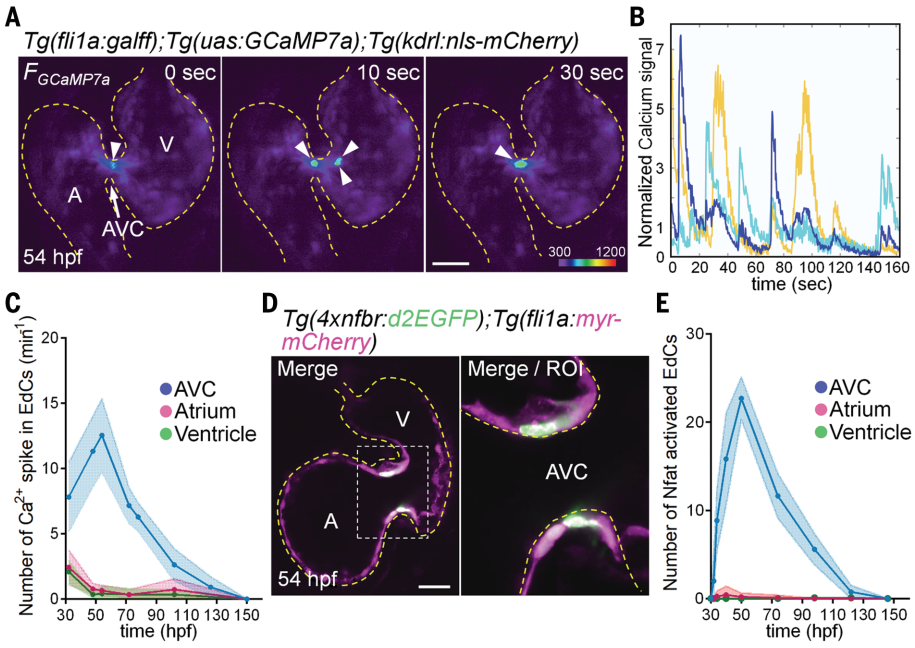

Fig. 1. Endogenous Ca^{2+} influx and Nfat signal activation occur in EdCs of the AVC during valvulogenesis. (**A**) Representative single-scan beating heart images of the *Tg(fli1a:galff);Tg(uas:GCaMP7a);Tg(kdrl:nls-mCherry)* embryo. Panels are the heatmap-colored GCaMP7a images at the indicated time points. Arrowheads and dashed lines indicate GCaMP7a signal and outline of the endocardium, respectively. (**B**) Normalized Ca^{2+} dynamics determined by $F_{GCaMP7a}/F_{nls\text{-}mCherry}$. Each colored line indicates the ratiometric change of individual cells (three cells) shown in movie S2. (**C**) The number of Ca^{2+} spikes in EdCs of the indicated region from 32 to 150 hpf ($n > 5$). (**D**) Confocal single-scanned heart images of *Tg(4xnfbr:d2EGFP);Tg(fli1a:myr-mCherry)* embryo ($n = 20$). (**E**) Number of Nfat reporter–activated EdCs from 30 to 146 hpf ($n = 14$). A, atrium; V, ventricle. Scale bars, 30 μm.

[1]Institut de Génétique et de Biologie Moléculaire et Cellulaire (IGBMC), Centre National de la Recherche Scientifique UMR7104, Institut National de la Santé et de la Recherche Médicale U1258 and Université de Strasbourg, Illkirch, France. [2]Department of Cell Biology, National Cerebral and Cardiovascular Center Research Institute, Suita, Japan. [3]Université de Paris, Centre National de la Recherche Scientifique UMR7592, Institut Jacques Monod, Paris, France. [4]Department of Biomedical Engineering, National University of Singapore, Singapore, Singapore. [5]Department of Bioengineering, Imperial College London, London, UK.
*Corresponding author. Email: jvermot@ic.ac.uk

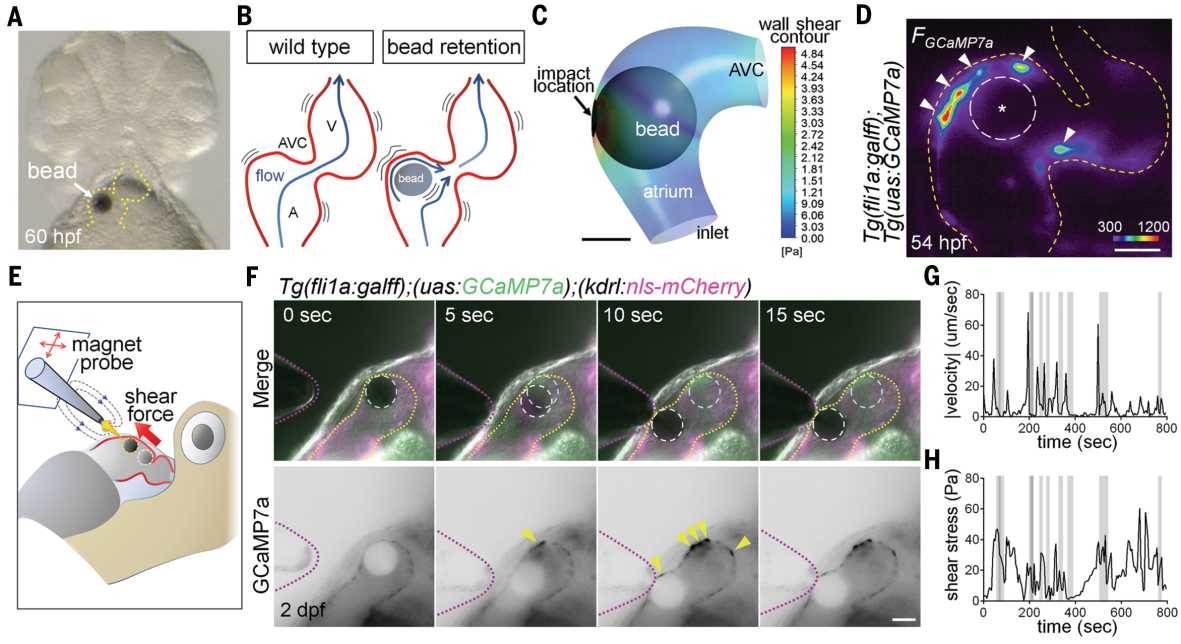

Fig. 2. Mechanical forces directly trigger Ca^{2+} influx in EdCs of zebrafish heart. (**A**) Representative image of bead implantation into the heart. (**B**) Schematics of bead retention. (**C**) Force intensities from 3D dynamic mesh simulation of wall shear stress with a bead (clear circle) close to the impact location. (**D**) Representative GCaMP7a image of embryo grafted with a bead (asterisk). (**E**) Schematic of magnetic tweezer–based force application to a zebrafish heart. (**F**) Single-scan images of *Tg(fli1a:galff);Tg(uas:GCaMP7a);Tg(kdrl:nls-mCherry)* grafted embryo (original bead position is indicated by dashed cyan circles) pulled by the magnetic probe (dotted magenta lines), left view (n = 6, yielding similar results). (**G** and **H**) Quantification of bead velocity (G) and shear stress (H) applied by the magnetic tweezer shown in movie S7. Gray shading indicates the period of activated GCaMP7a signal in EdCs. Arrowheads indicate the GCaMP7a signal and yellow dashed lines the endocardium. Scale bars, 15 μm in (C) and 30 μm in (D) and (F).

bead into the cardiac lumen by microsurgery without perturbing heart function (Fig. 2, A and B, and movie S3). To quantify the force generated around the bead, we performed a three-dimensional (3D) simulation of the wall shear stress and pressure around the bead using an image-based computational fluid dynamics simulation with dynamic wall motion (*15*) (Fig. 2C and fig. S4, A to C). Shear stress and pressure were increased in the vicinity of the bead (movie S4) and were close to the endogenous forces generated where the valve normally forms (*15*–*17*). In vivo, we observed Ca^{2+} spikes in the EdCs next to the bead when trapped in the atrium or in the ventricle (Fig. 2D; fig. S4, D to G; and movies S5 and S6). To more precisely control shear forces, we directly manipulated the bead within the heart using magnetic tweezers (Fig. 2E). The force generated ranged from 100 to 2000 pN (fig. S4, H and I), a stimulus that is slightly higher than endogenous wall shear stresses generated in the AVC (*15*–*17*). Although the magnet probe alone did not affect Ca^{2+} influx in EdCs, direct pulling of the magnetic bead led to the generation of Ca^{2+} influx in the EdCs of the arrested heart (Fig. 2, F to H; fig. S4, J and K; and movie S7). Thus, Ca^{2+} fluxes are induced in the EdCs by wall shear stress and associated wall pressure, whereas cardiac contractility is not necessary.

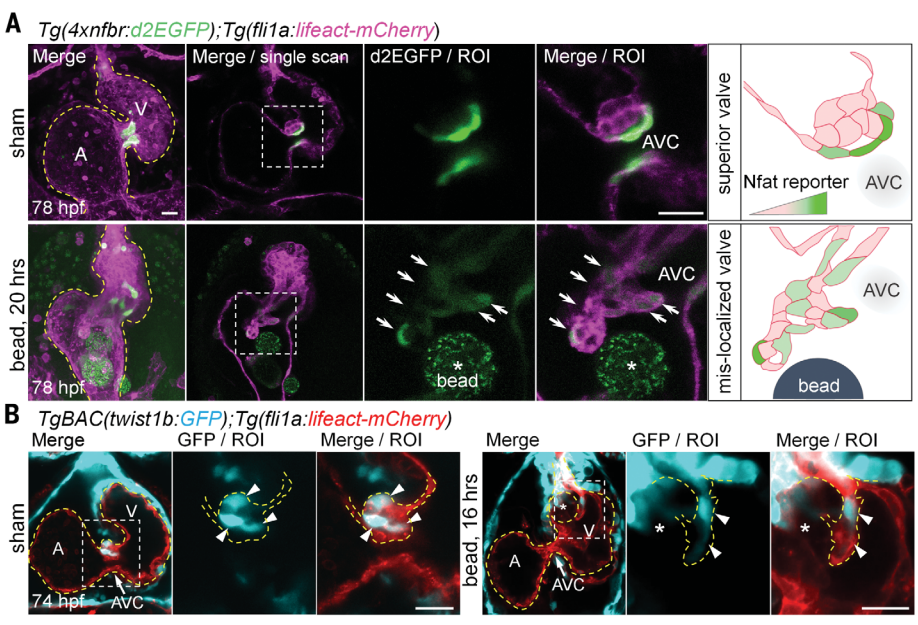

Fig. 3. Artificial forces lead to the formation of ectopic valve–like structures. (**A**) Confocal images of *Tg(4xnfbr:d2EGFP);Tg(fli1a:lifeact-mCherry)* embryo after sham treatment (n = 11) and 20 hours after bead grafting (n = 8) with the schematics of superior valve (top) and mislocalized valve (bottom) with Nfat reporter intensity (n > 5, yielding similar results individually). Arrows indicate the ectopic structure. (**B**) Representative confocal images of *TgBAC(twist1b:GFP);Tg(fli1a:lifeact-mCherry)* embryo after sham treatment (n = 10) and 16 hours after bead grafting (n = 7). Arrowheads indicate Twist1b expression in EdCs, yellow dashed lines the outline of the endocardium, and asterisks and dashed circles the grafted bead. Scale bars, 20 μm.

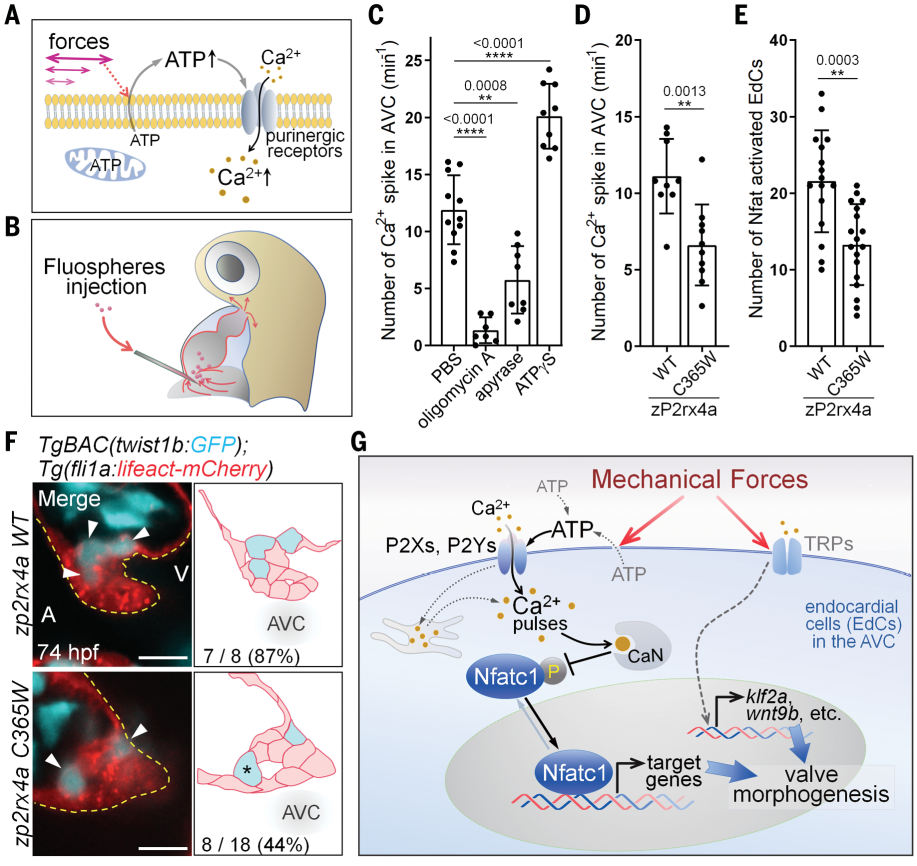

Fig. 4. Extracellular ATP and P2rx channels function for valve development. (**A**) ATP-dependent P2XRs Ca^{2+} activation schematic. (**B**) Schematic of the microinjection approach to injecting drugs into cardiac lumen. (**C**) Number of Ca^{2+} spikes in EdCs of the AVC for PBS-injected (n = 11), oligomycin A–injected (n = 7), apyrase-injected (n = 8), and ATPγS-injected (n = 9) embryos at 54 hpf. (**D** and **E**) Number of Ca^{2+} influxes (D) and Nfat reporter activation (E) in EdCs of the AVC for embryos injected with *zp2rx4aWT* [n = 9 in (D) and n = 16 in (E)] and *zp2rx4aC365W* mRNA [n = 10 in (D) and n = 18 in (E)] at 54 hpf. (**F**) Confocal images of *TgBAC(twist1b:GFP);Tg(fli1a:lifeact-mCherry)* embryo injected with *zp2rx4aWT* (n = 8) and *zp2rx4aC365W* mRNA (n = 18). Arrowheads and percentages indicate *twist1b* expression in the EdCs and occurrence of each representative valve structure, respectively. Asterisks indicate mislocalized EdCs with ectopic *twist1b* expression. (**G**) Summary of endocardial mechanosensitive signal pathways for valve development. Note that forces trigger the ATP-transducer (Ca^{2+})-decoder (NFAT) system, which is independent of the *klf2a* expression activation. Scale bars, 15 μm.

We assessed the biological relevance of the localized response initiated by bead grafting to find out whether it is associated with the formation of ectopic valves. Sixteen to 20 hours after bead grafting in the atrium, valve-like EdC clusters were observed near the bead. The valve-like structures were visible in the atrial region that protruded from the atrial surface to the atrial cavity or the cardiac jelly (Fig. 3A and fig. S5A). A grafted bead triggered the mislocalized protrusions into cardiac jelly (fig. S5A), which constitutes the first sign of valve morphogenesis in zebrafish (*18*). We additionally found that the grafted bead induced the expression of *twist1b* in the valve-like structures (Fig. 3B and fig. S6, A to D) and the ectopic expression of *klf2a*, *klf4a*, and *wnt9b* in the EdCs surrounding it (fig. S7, A to C and F). These observations indicate that ectopic valve–like structures share similarities with endogenous valves. In addition, Nfat activity was ectopically induced in EdCs located near the bead (fig. S5, B and C), which is consistent with the fact that Nfatc1 nuclear localization is activated in response to ectopic forces and reduced when heart contractility is affected (fig. S5, D to G). Nuclear translocation of Nfatc1 was inhibited by a chemical blocker of calcineurin (FK506) acting on the Ser/Thr dephosphorylation site of Nfat (fig. S5D). Thus, the nuclear localization of Nfatc1 is promoted by increased mechanical force in a Nfatc1 Ser/Thr dephosphorylation–dependent manner. Neither *klf2a* nor *klf4a* expression was affected when calcineurin was inhibited by either FK506 or VIVIT, a selective peptide inhibitor of Nfat (*19*) (fig. S7, C to F), suggesting that the Ca^{2+}-Nfat signaling pathway acts independently of the *klf2a* mechanotransduction pathway. Conversely, *egr1*, a known mechanosensitive gene expressed in the AVC (*20*), was down-regulated by calcineurin inhibition (fig. S7, G and H), suggesting that *egr1* acts downstream of Nfatc1. Thus, mechanical forces are key to specifying heart valve position during development by modulating both the Klf2a- and the Nfatc1-signaling pathways.

To characterize the factors responsible for the force-dependent Ca^{2+}-Nfat signal activation, we first focused on established mutant lines for the stretch-sensitive channels Trpp2, Trpv4, Piezo1, Piezo2a, and Piezo2b (*17*, *21*, *22*) and for ciliogenesis (*iguana*, Dzip1) (*23*), which have been implicated in flow sensing in the cardiovascular system (*24*). We found that all of these mutants showed normal Ca^{2+} activation (fig. S8, A and B) as well as for embryos treated with gadolinium ion (Gd^{3+}), a nonspecific stretch-sensitive channel blocker (fig. S8C). Alternatively, ATP is released in cultured endothelial cells in response to mechanical stimuli (*25*). As a response, ATP activates Ca^{2+} signaling through the purinergic receptor P2X channels (*26*) (Fig. 4A). Accordingly, Ca^{2+} influx in EdCs of the AVC was abolished when cytosolic ATP levels were depleted by oligomycin A, a mitochondrial ATP synthase inhibitor (fig. S8D). We investigated whether extracellular ATP alters Ca^{2+} influx in EdCs by microinjecting oligomycin A, apyrase (an ATPase), and ATPγS (an ATP analog) into the cardiac lumen (Fig. 4B, and movie S8), and found that the Ca^{2+} influx was significantly affected in response to changes in extracellular ATP levels (Fig. 4C and fig. S8, E to I). Transcripts of the ATP receptors *p2rx1*, *p2rx4a*, and *p2rx7* were present in EdCs of the heart (fig. S9, A and B). Embryos treated with antagonists of P2X1, P2X4, and P2X7; embryos overexpressing a dominant-negative form of either human *P2X4* (*hP2X4C353W*) or zebrafish *p2rx4a* (*zP2rx4aC365W*) mRNA; and *p2rx4a* morphants displayed a significant reduction of Ca^{2+} spikes in EdCs (Fig. 4D and fig. S9, C to G and I). These results show that the Ca^{2+} influx in EdCs is modulated by P2X channels in response to changes in extracellular ATP levels.

We next assessed whether the activation and inhibition of P2X-mediated ATP signaling affected valve formation. Embryos treated with a combination of P2X1, P2X4, and P2X7 antagonists; a combination of P2X4 with P2Y2 antagonists; a P2X4 antagonist; or a P2Y2 antagonist suppressed Nfat reporter activation, whereas the other P2X or P2Y antagonists had no effect (fig. S10, A and B). Furthermore, overexpression of a dominant-negative form and knock-down of *p2rx4a* did not affect *klf2a* and *klf4a* expression but significantly suppressed Nfat reporter expression (Fig. 4E and fig. S9, H, J, and K), correlating well with the abnormal Ca^{2+} activation (Fig. 4D and fig. S9G). In addition, embryos displayed abnormal valve

structures with incomplete morphogenesis of the valve, absence of leaflet formation (Fig. 4F), and mislocalized Twist1b-positive cells in the endocardium when *p2rx* function was inhibited (Fig. 4F and fig. S11, A to C). EdCs were excluded from the luminal part of the valve when Nfat activity was suppressed in these cells (fig. S11, D and E), consistent with the fact that Nfatc1 is necessary for valve development in zebrafish (*7*). Although vascular endothelial growth factor (Vegf) signaling is known to activate Nfat signaling (*27*), a Vegfr2 inhibitor had no effect on either Nfat reporter expression or Ca^{2+} activation in the EdCs (fig. S10, A to D). These results suggest that P2X and P2Y receptors coordinately modulate Nfat activity in the EdCs independently of VEGF signaling. In addition, we found that Nfat activity in the endocardium seemed to be unrelated to tyrosine phosphorylation (*28*) (fig. S10, A and E). Altogether, these results confirm that P2X functions act upstream of Nfat activity to control valve development in response to mechanical stimuli.

Mechanical forces have been implicated in a broad range of events during embryonic development (*29*–*31*). The presented work reframes our view of how EdCs interpret mechanical forces (Fig. 4G) and supports the intriguing possibility that valve formation is mainly defined by the mechanosensitive inputs resulting from the local tissue constraints and flow forces (*7*, *18*, *32*–*34*). Piezo and Trp channels are well-established stretch-sensitive channels involved in cardiovascular morphogenesis and valve development (*17*, *21*, *35*–*37*). Our work identifies ATP as an additional mechanosensitive paracrine signal by which hemodynamic forces can direct heart valve development. Therefore, it is a compound that could be used to help grow heart valves in vitro and may be involved in congenital heart valve defects. More generally, this work shows that biological systems rely on multiple mechanosensitive pathways to precisely control morphogenetic processes. ATP release and stretch-sensitive channels are activated in response to discrete mechanical stimuli to precisely generate the permissive signal controlling the localization and timing of valve morphogenesis. We view this as a safeguard mechanism that increases the robustness of the mechanosensitive process to avoid ectopic valve formation in other regions of the heart where mechanical forces are also at work.

REFERENCES AND NOTES

1. E. Steed, F. Boselli, J. Vermot, *Biochim. Biophys. Acta* **1863**, 1760–1766 (2016).
2. A. L. Duchemin, H. Vignes, J. Vermot, R. Chow, *Curr. Opin. Genet. Dev.* **57**, 106–116 (2019).
3. A. Paolini, S. Abdelilah-Seyfried, *Curr. Opin. Cell Biol.* **55**, 52–58 (2018).
4. F. Boselli, J. B. Freund, J. Vermot, *Cell. Mol. Life Sci.* **72**, 2545–2559 (2015).
5. Y. Yokota *et al.*, *eLife* **4**, e08817 (2015).
6. C. P. Chang *et al.*, *Cell* **118**, 649–663 (2004).
7. F. Gunawan, A. Gentile, S. Gauvrit, D. Stainier, A. Bensimon-Brito, *Circ. Res.* (2020).
8. A. M. Ranger *et al.*, *Nature* **392**, 186–190 (1998).
9. B. Zhou *et al.*, *Development* **132**, 1137–1146 (2005).
10. R. A. Schulz, K. E. Yutzey, *Dev. Biol.* **266**, 1–16 (2004).
11. B. Wu, H. S. Baldwin, B. Zhou, *Trends Cardiovasc. Med.* **23**, 294–300 (2013).
12. F. Boselli, E. Steed, J. B. Freund, J. Vermot, *Development* **144**, 4322–4327 (2017).
13. J. Vermot *et al.*, *PLOS Biol.* **7**, e1000246 (2009).
14. S. E. Lyons *et al.*, *Proc. Natl. Acad. Sci. U.S.A.* **99**, 5454–5459 (2002).
15. Y. Y. Foo *et al.*, *Biomech. Model. Mechanobiol.* **19**, 221–232 (2020).
16. F. Boselli, J. Vermot, *Methods* **94**, 129–134 (2016).
17. E. Heckel *et al.*, *Curr. Biol.* **25**, 1354–1361 (2015).
18. E. Steed *et al.*, *Nat. Commun.* **7**, 11646 (2016).
19. J. Aramburu *et al.*, *Science* **285**, 2129–2133 (1999).
20. T. Banjo *et al.*, *Nat. Commun.* **4**, 1978 (2013).
21. A. L. Duchemin, H. Vignes, J. Vermot, *eLife* **8**, e44706 (2019).
22. J. Schottenfeld, J. Sullivan-Brown, R. D. Burdine, *Development* **134**, 1605–1615 (2007).
23. K. Sekimizu *et al.*, *Development* **131**, 2521–2532 (2004).
24. P. Campinho, A. Vilfan, J. Vermot, *Front. Physiol.* **11**, 552 (2020).
25. K. Yamamoto *et al.*, *J. Cell Sci.* **124**, 3477–3483 (2011).
26. K. Yamamoto, R. Korenaga, A. Kamiya, J. Ando, *Circ. Res.* **87**, 385–391 (2000).
27. A. L. Armesilla *et al.*, *Mol. Cell. Biol.* **19**, 2032–2043 (1999).
28. A. K. Patra *et al.*, *Nat. Immunol.* **14**, 127–135 (2013).
29. C. P. Heisenberg, Y. Bellaïche, *Cell* **153**, 948–962 (2013).
30. T. Mammoto, D. E. Ingber, *Development* **137**, 1407–1420 (2010).
31. T. Merle, E. Farge, *Curr. Opin. Cell Biol.* **55**, 111–118 (2018).
32. S. Donat *et al.*, *eLife* **7**, e28939 (2018).
33. F. Gunawan *et al.*, *J. Cell Biol.* **218**, 1039–1054 (2019).
34. J. Pestel *et al.*, *Development* **143**, 2217–2227 (2016).
35. J. Li *et al.*, *Nature* **515**, 279–282 (2014).
36. K. Nonomura *et al.*, *Proc. Natl. Acad. Sci. U.S.A.* **115**, 12817–12822 (2018).
37. S. S. Ranade *et al.*, *Proc. Natl. Acad. Sci. U.S.A.* **111**, 10347–10352 (2014).

ACKNOWLEDGMENTS

We thank the members of J.V.'s and N.Mo.'s laboratories; the imaging and the fish facility staff of IGBMC; and M. Sone, A. Chiba, K. Hiratomi, and T. Babazono in N.Mo.'s laboratory for their assistance. **Funding:** This work was supported by the European Research Council (GA no. 682938), the Agence Nationale de la Recherche (ANR-15-CE13-0015-01, ANR-10-IDEX-0002–02, ANR-12-ISV2-0001-01, and ANR-10-LABX-0030-INRT to J.V.), the University of Strasbourg (USIAS-2017-097), the Takeda Medical Research Foundation, the Uehara Memorial Foundation, the Cell Science Research Foundation (H.F.), and JSPS KAKENHI (21K 06764 to H.F.). R.W.-Y. C. was supported by a Fondation Lefoulon-Delalande fellowship. J.X. acknowledges a fellowship from the Chinese Scholarship Council (201708070046) and N.Mi grants from La Ligue Contre le Cancer (EL2021.LNCC/ NiM) and the European Research Council (ERC CoG "Forcaster" no. 647073). **Author contributions:** H.F. and J.V. conceived the project. H.F. designed the work and performed experiments. R.W.C. performed the analysis of Ca^{2+} signaling normalization. H.F., J.X. and N.Mi. performed the magnetic tweezer experiments. Y.Y.F. and C.H.Y performed the analysis of 3D simulation. N.Mi. and N.Mo. provided reagents and suggestions. H.F. and J.V. wrote the manuscript. All authors interpreted the data, contributed to data analysis, and discussed the manuscript. **Competing interests:** The authors declare no competing financial interests. **Data and materials availability:** All data are available in the main text or the supplementary materials. Transgenic lines are available upon request.

SUPPLEMENTARY MATERIALS

science.org/doi/10.1126/science.abc6229
Materials and Methods
Figs. S1 to S11
Captions for Movies S1 to S8
References (*38*–*56*)
Movies S1 to S8
MDAR Reproducibility Checklist

View/request a protocol for this paper from *Bio-protocol*.

4 May 2020; accepted 31 August 2021
10.1126/science.abc6229

Bioelectric signaling and the control of cardiac cell identity in response to mechanical forces

Hajime FukuiRenee Wei-Yan ChowJing XieYoke Yin FooChoon Hwai YapNicolas MincNaoki MochizukiJulien Vermot

Science, 374 (6565), • DOI: 10.1126/science.abc6229

Making cardiac valves via mechanical forces

Cardiac valves form in response to mechanical forces generated by the beating heart. Fukui *et al*. studied how patterning signals are generated in response to these forces (see the Perspective by Jain and Epstein). They show that two mechanotransduction pathways act in parallel to instruct cardiac valve progenitors: a well-established transient receptor potential mechanosensation pathway and an extracellular ATP-dependent purinergic receptor pathway that triggers Ca oscillations and results in nuclear translocation of the protein nuclear factor of activated T cells 1. These two synergistic mechanotransduction pathways generate positional information and control valve formation. The use of multiple pathways may be a general mechanism used by mechanosensitive biological systems to increase the robustness and precision of mechanotransduction. —BAP